PHYSICS

Measurement-induced photonic topological insulators

Quancheng Liu[1]†, Weijie Liu[1]†, Yuechen Jia[1], Klaus Ziegler[2], Andrea Alù[3,4]*, Feng Chen[1]*

Topological order in photonics, defined by pseudo-spin degrees of freedom, is traditionally static. By contrast, a unique quantum effect is that measurements alter system states. The convergence of these foundational concepts—measurement and topology—remains unexplored. Here, we demonstrate that topological order can be dynamically modified by repeated measurements. By fabricating a photonic lattice composed of an array of contiguous waveguides and incorporating 16,800 appended waveguide segments as discrete, nonindependent units, we established a classical-wave platform simulating the backaction from measurements and observed measurement-induced topological order in photonic lattices. Beyond topology, we further demonstrate that measurements can universally control the lattice by tailoring its Hilbert space and validate experimentally. Our study not only offers a quantum approach to dynamically tailor topological order but also unveils measurements as a powerful universal control tool, paving the way to on-chip topological materials and measurement-induced control over photonic systems.

INTRODUCTION

Topological insulators are a phase of matter that supports robust transport along boundaries, yet it forbids propagation in the bulk (*1*). They have sparked an active field of research, spanning multiple disciplines, with applications going from robust spintronic devices to fault-tolerant quantum computing. In this context, the quantum Hall effect, induced by an external magnetic field, has showcased a first popular example of how topological transport can be induced in practical physical systems (*2*). Subsequently, the quantum spin Hall effect has revealed that topology can arise without external magnetic bias, driven by spin-orbit coupling (*3*–*5*). Experimental verification of these phenomena has been achieved across various platforms (*6*–*11*). Specifically, the realization of topological phenomena in photonics has been extensively investigated (*12*–*18*), leading to exotic findings, such as topological lasers (*19*, *20*), non-Hermitian topological physics (*21*), and nonlinearity-induced topology (*22*). Recently, Floquet engineering, involving time-dependent coupling elements, has emerged as a powerful tool for manipulating the topological order, both theoretically and experimentally, unveiling additional degrees of freedom for the generation of topological insulators (*23*–*31*) and demonstrating enhanced robustness (*32*).

Measurements are at the basis of the observation of natural phenomena in any physical system. In the realm of quantum physics, the measurement of a quantum system inevitably alters its state, a phenomenon known as measurement backaction (*33*, *34*). Such features are harnessed, for example, in quantum information science, where measurements are crucial for entanglement phase transitions, quantum error correction, and measurement-based computation (*35*–*42*). Notably, conducting rapid, stroboscopic measurements on a system can induce the quantum Zeno effect, whereby the evolution of a system is suppressed by the backaction of the measurements, maintaining its initial state (*43*). This effect is the quantum analog of Zeno's paradox, which claims that an arrow in flight may be deemed motionless when observed at any specific instant in time (*44*, *45*). Notably, the physical observable measured here is the particle density within specific states. However, the primary objective of these measurements is not to obtain values of the observables themselves but rather to use the measurement-induced backaction to modify the evolution of the system (*46*, *47*). Intriguingly, recent studies have shown that the quantum Zeno effect does not simply halt the system evolution; rather, the Zeno dynamics confine this evolution to a specific subspace of the entire Hilbert space, with frequent measurements delineating the boundaries of the evolution space (*48*). Experimental observations of the quantum Zeno effect have been reported across various physical platforms, including atomic (*49*, *50*), optical (*51*–*56*), and acoustic (*57*, *58*) systems. In an experimental validation, the crucial issue remains to realize the measurement's backaction on the system. In such a feat, the observer-system quantum entanglement is unnecessary, because the ultimate effect of measurements is to induce a change in the state of the system. This methodological approach is well established in the existing literature for the investigation of the quantum Zeno effect (*49*–*58*). Notably, by leveraging the quantum-optical analogy, i.e., the mapping between the Schrödinger equation for quantum waves and the paraxial Helmholtz equation for classical light waves—an effective framework for exploring various quantum phenomena (*59*, *60*)—the optical Zeno effect has been observed in classical photonic lattices (*51*, *53*–*56*).

These studies have demonstrated that measurements can alter the evolution of a system. However, merely freezing the evolution or confining it to a specific subspace can difficultly yield meaningful physical insights or practically useful phenomena. Here, we explore whether the backaction of measurements can modify the topological order of a photonic structure and induce a topological transition. This study not only examines the phenomenon of the measurement-induced Zeno effect, but it is also relevant to the design of dynamic topological insulators, where the topological order is generated through external operations. Developing different mechanisms for generating topological phases of matter—such as external magnetic fields, spin-orbit coupling, or nonlinearity—is a central challenge in topological physics. Thus, could a series of measurements enable such a mechanism?

In the following, we theoretically and experimentally demonstrate a measurement-induced photonic topological insulator, establishing a direct connection between measurement and the topology of

[1]School of Physics, State Key Laboratory of Crystal Materials, Shandong University, Jinan 250100, China. [2]Institut für Physik, Universität Augsburg, D-86135 Augsburg, Germany. [3]Photonics Initiative, Advanced Science Research Center, City University of New York, New York, NY 10031, USA. [4]Physics Program, Graduate Center, City University of New York, New York, NY 10016, USA.
*Corresponding author. Email: aalu@gc.cuny.edu (A.A.); drfchen@sdu.edu.cn (F.C.)
†These authors contributed equally to this work.

matter. Specifically, by emulating the backaction of measurements in the Zeno regime using a classical photonic platform, we drive a topologically trivial Lieb lattice into a topological phase, demonstrating unidirectional edge transport and an insulating bulk. Unlike conventional Zeno phenomena, in which the measured states are static, we design different measurement projectors in a time-dependent fashion, which dynamically slice the Hilbert space of the lattice (see theoretical derivations with standard quantum projective measurements in Supplementary Text S1 and table S1), resulting in a modified anomalous Floquet topological insulator platform (*23*). In photonics, measurement-induced quantum phenomena can be investigated classically by leveraging quantum-optical analogy experiments, where optical modes correspond to distinct quantum states and their temporal evolution is mapped into spatial propagation (*51*, *53*–*56*). Typically, a measurement involves coupling a measurement apparatus to the monitored system, resulting in measurement backaction. A primary experimental challenge is designing the system-measurement interaction to achieve the desired outcomes within a photonic framework, particularly when dealing with a large number of measurements. In our experiments, we do not implement genuine quantum measurements featuring observer-system entanglement; instead, the measurements are executed using built-in, on-demand segmented waveguide sections that induce periodic modifications to the guided light fields, effectively mimicking the backaction of repeated quantum measurements and realizing the optical analog of the Zeno effect on the photonic lattice. Notably, despite the inherent loss associated with each individual measurement, light propagation within the photonic lattice remains unitary, protected by the optical Zeno effect. We further demonstrate that by engineering noncommutative Zeno subspaces, the evolution of light across the photonic lattice can be precisely controlled in an on-demand fashion. As a further proof of the opportunities enabled by this concept, we experimentally implement three-level Zeno subspaces, effectively creating in-lattice beam splitters within the Lieb lattice.

RESULTS

Generating the backaction of stroboscopic measurements in photonics

In the tight-binding approximation, the evolution of light in a two-dimensional photonic lattice is described by the discrete paraxial Helmholtz equation

$$i\frac{d}{dz}\psi_n(z) = \beta_n(z)\psi_n(z) + \sum_{\langle n,m\rangle}\kappa_{m,n}(z)\psi_m(z) \equiv H(z)\psi_n(z) \quad (1)$$

where $\psi_n(z)$ is the electric field amplitude at lattice node n; $\kappa_{m,n}(z)$ is the hopping strength between waveguides m and n; $\beta_n(z)$ is the propagation constant, which is the same for all sites; and the summation is taken over neighboring waveguides. This equation formally resembles the Schrödinger equation, with light propagation along z playing the role of time. Hence, a longitudinal modulation of the waveguide emulates the temporal evolution of the associated Hamiltonian, enabling the implementation of measurement backaction to the lattice using a prefabricated photonic system that varies along z. In our experiments, we use femtosecond laser direct writing (*61*) on glass wafers to fabricate single-mode waveguide structures (see Materials and Methods). We arrange straight waveguides to construct a photonic Lieb lattice (*62*): The lattice geometry is formed by arranging evanescently coupled straight waveguides of length L into unit cells with one central site and two peripheral sites of 11 μm in distance, aligned along orthogonal axes (Fig. 1, A and B). The Lieb lattice is topologically trivial and features a flat band. The key challenge lies in implementing the analog of Zeno measurements to introduce tailored broken symmetries that induce a topological transition.

In our experimental protocol, measurements at specific lattice nodes are mapped onto waveguide connections appended to these nodes (illustrated in Fig. 1, A and B). Here, the physical observable is the light intensity at the nodes. However, as mentioned, the goal of the measurements is not to obtain the light intensity itself but rather to induce the optical Zeno effect through measurement backaction. Each waveguide connection segment acts as a measurement apparatus $\mathcal{M}$ coupled to the nearest straight waveguide (see further details and a non-Hermitian model in Supplementary Text S2). As shown in Fig. 1A, the system-measurement interaction time is determined by the segment length l, which can be adjusted. In the gap between the segments of length g, the coupling vanishes. Light can propagate out of the system from the gap between the segments, and photons are emitted, corresponding to the readout process. Hence, the waveguide segment, together with the gap, emulates a complete measurement process on the adjacent straight waveguide. A similar protocol to realize the backaction of measurements and the Zeno effect was used in ^{87}Rb (*46*), where the waveguide segments represent distinct energy levels, and the laser pulse duration is analogous to the segment length l. The optical Zeno effect emerges in long interaction times between the segments and the monitored node with $l = 170$ μm and $g = 30$ μm (see additional experiments in Supplementary Text S3 and S4). In the Zeno limit, the couplings between measured and surrounding nodes are restricted to specific values that prevent light from hopping to the measured node.

This construct implements the optical Zeno effect for a single node in the lattice. More generally, the backaction of measurements can restrict the evolution of the system to a subspace of the system's Hilbert space (*42*, *45*–*47*). This subspace is called the Zeno subspace. As a simple example, consider a five-site chain where the middle site (site 3) is measured. This measurement decouples site 3 from the system and leads to the formation of two Zeno subspaces, each consisting of two sites (sites 1 and 2, and sites 4 and 5, respectively.) (see Supplementary Text S1 for more details). Returning to our lattice model, by selectively measuring different nodes in the Lieb lattice (represented as blue sites in Fig. 1C), we can modify the lattice symmetry ad hoc. For instance, we can purposely inhibit inter- and intracell couplings using the Zeno effect and only allow exclusive hopping between the two yellow nodes in the unit cell. These yellow nodes represent the Zeno subspace formed on the Lieb lattice because of the Zeno effect, which confines the particle's evolution to this subspace rather than the full Hilbert space. For instance, in step 1, Zeno measurements on nodes C, D, E, and F inhibit all other couplings in the unit cell; as a result, particle hopping is restricted solely between nodes A and B (Fig. 1, B and C). This happens because the backaction of measurements on nodes C to F effectively suppresses the transitions to these nodes; consequently, we get a Zeno subspace formed only by nodes A and B. Physically, the ensemble of measured states $|d\rangle$ defines the projection operator $P = I - \sum_d |d\rangle\langle d|$, where I is the identity matrix of order six. Consequently, the backaction of these measurements restricts the evolution of the system into

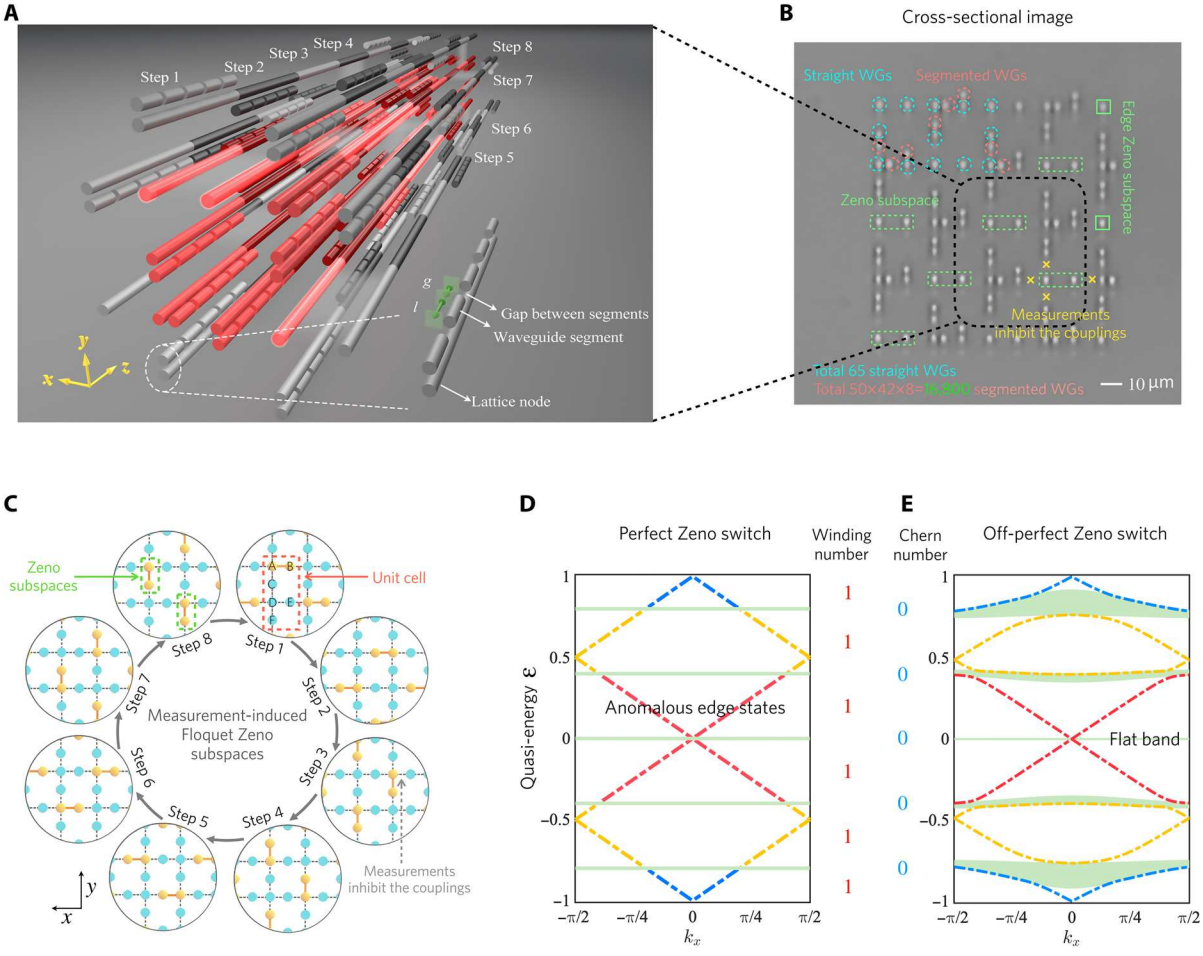

Fig. 1. Photonic implementation of a measurement-induced topological insulator. (**A**) Schematic illustration showing how the backaction of measurements and Floquet driving protocol are implemented using 3D waveguide arrays with waveguide segments and gaps. Here, only part of the lattice structure is presented, and the full lattice image is shown in (B). (**B**) Experimental cross-sectional image of Floquet step 1, fabricated using femtosecond laser writing. We fabricate a total of 65 straight waveguides (WGs) and 16,800 segmented waveguide portions to experimentally realize the measurement-induced topological insulator. (**C**) Measurement-induced eight-step Floquet driving protocol. The measured sites are marked in blue, and the nonmeasured sites are marked in yellow, which constitute the Zeno subspace generated by measurements for each step. (**D** and **E**) Quasi-energy ε spectrum as a function of the quasimomenta k_x for the perfect Zeno switching (experimentally realized) and off-perfect Zeno switching scenarios. The spectrum of the measurement-induced topological insulator features a zero net Chern number for each bulk band and anomalous edge modes characterized by a nonvanishing winding number.

a particular Zeno subspace and the corresponding Zeno subspace Hamiltonian reads $H_p(k) = PH(k)P$. Hence, the original lattice Hamiltonian $H(k)$ is transformed into a modified Hamiltonian, $H_p(k)$ (further theoretical derivations in Supplementary Text S1 and table S1). In the theoretical framework, each measurement can either succeed (measuring the system within the Zeno subspace) or fail (projecting it into the orthogonal subspace). In the Zeno limit, where measurements are performed frequently, the probability of any failed measurements vanishes, and all the measurements are successful with certainty (see Supplementary Text S1 for details). Therefore, the Zeno effect is a deterministic phenomenon that naturally emerges under frequent measurements (*42*, *45*). $H_p(k)$ describes the Zeno subspace for the measured Lieb lattice in the momentum space, and the evolution inside this subspace is the Zeno dynamics, as $\dim[H_p(k)] > 1$. In step 1, the measurement projection operator $P_1 = I - \sum_{d=\mathrm{C,D,E,F}} |d\rangle\langle d|$, which describes Zeno measurements on nodes C to F. Consequently, the Zeno subspace for step 1 is $H_p^1(k) = P_1 H(k) P_1 = |\mathrm{A}\rangle\langle\mathrm{B}| + |\mathrm{B}\rangle\langle\mathrm{A}|$. In this case, when injecting a laser beam from site A, the light no longer spreads across the entire photonic Lieb lattice; instead, it exhibits Rabi oscillations (*63*, *64*) between nodes A and B, characterized by the periodic and coherent transfer of light between the two coupled waveguides, resulting in an oscillatory exchange of optical intensity between the sites.

Floquet Zeno subspaces

Our measurement-induced topological photonic insulator uses a cyclically arranged Floquet eight-step driving protocol (Fig. 1C). The complete Floquet cycle spans a total duration L, with each step being $L/8$. The timing of these steps is controlled by the number of

measurements N in our experiment, i.e., $L/8 = N(l+g)$. At each distinct propagation step X, we design the measured states to realize a unique Zeno subspace $H_p^X(k)$ (explicit expressions in Supplementary Text S1 and table S1). This setup guarantees exclusive routing of light from each waveguide to its designated nearest neighbor. By systematically inducing eight distinct Zeno subspaces in sequence, we realize an anomalous Floquet topological insulator. Notably, the Floquet topological insulator induced by such measurements exhibits a higher degree of sparsity compared to the conventional scenario, necessitating additional nodes for the measurement process. The overall dynamics of the system through one complete cycle are governed by the Floquet operator

$$U(L) = \mathcal{T}\exp\left[-i\int_0^L dtH(k,t)\right] = \prod_{X=1}^{8}\exp\left[\frac{-iH_p^X(k)L}{8}\right] \quad (2)$$

where $\mathcal{T}$ denotes the time ordering, and $H_p^X(k)$ represents the measurement-induced Zeno subspace. The quasi-energy ε is defined through the eigenvalue equation of the Floquet operator $U(L)$, which satisfies $\phi(L) = U(L)\phi(0) = e^{-i\varepsilon L}\phi(0)$, with ϕ being the Floquet eigenstate (*29*). Hence, the quasi-energy ε exhibits periodicity of $2\pi/L$. We analyze the bulk band structure as a function of the quasi-momentum k_x for different driving periods L by changing the measurement durations. The scenario wherein light completely transitions between waveguides in each Zeno subspace within one cycle forms the "perfect Zeno switch." This case involves 50 measurements at each node per cycle. The "off-perfect Zeno switch" scenario, where only partial light transition occurs, involves 40 measurements at each node. The quasi-energy ε spectrum, illustrated in Fig. 1 (D and E), reveals the emergence of topological edge states, characterized by a nontrivial winding number $\mathcal{W} = 1$. Notably, the absence of a Chern number ($C = 0$) suggests an unconventional topological response. Instead, the presence of a nonvanishing winding number, counting the edge states that cross a particular bandgap, indicates that the system topological properties stem from its dynamic evolution, which is induced by the Zeno measurement process. Consequently, the measurement-induced lattice does not exhibit Chern-type topological insulator features but rather realizes an anomalous topological insulator with edge modes, driven by our measurement-induced Floquet protocol.

To experimentally observe the measurement-induced topological insulator, we fabricated a photonic Lieb lattice featuring 65 straight waveguides arranged to form a 4 by 4 square configuration, as shown in the cross-sectional micrograph in Fig. 1B. Following the creation of this lattice, we proceed with conducting measurements. To enable Zeno measurements, we introduce segmented waveguide sections into the system. We perform 50 measurements for each straight waveguide in a single step. In each step, 42 waveguides are measured, establishing the necessary Zeno subspaces to control light propagation within the lattice. The complete Floquet driving sequence consists of eight steps, resulting in the fabrication of 16,800 segmented waveguides, which correspond to the same number of measurements on the photonic Lieb lattice.

In the first set of experiments, a laser beam at a 532-nm wavelength was used to excite an internal site within the monitored lattice, as illustrated in Fig. 2A. Following four-step Zeno measurements, light propagation across the lattice was experimentally monitored. During each measurement step, the optical Zeno effect confines light within a two-level Zeno subspace, causing it to deterministically transition to the adjacent site. This resulted in a well-defined propagation path A → B → D → F → A, where the later sites D, F, and A belong to the next unit cell. After four steps, the light beam was entirely localized at the diagonally opposite site from the initial injection point, as shown by our experimental measurements in Fig. 2B. Subsequently, light was allowed to propagate for another four steps, moving from A to E and then to D and C and returning to A, as shown in Fig. 2C. The experimentally observed light distribution after eight steps is shown in Fig. 2D, where the light beam returns to its initial injection site, consistent with our theoretical predictions. These experiments illustrate that the backaction of measurements confines light propagation within the lattice within chiral loops, with an insulating response in bulk. For comparison, experiments without Zeno measurements correspond to a straight waveguide array lacking segmented sections. The laser is directed to the same site, allowing the light to disperse freely over a 4-cm distance. The resulting light distribution, shown in Fig. 2F, demonstrates the spread of light across the entire lattice. The distinct contrast in light distribution patterns between Fig. 2 (B, D, and F) highlights that the insulating properties of the lattice are induced by the Zeno measurement process.

Measurement-induced topological chiral edge transport and its robustness

We further investigate measurement-induced topological edge transport by directing a laser beam from the edge of the lattice, as illustrated in Fig. 3A. Initially, light travels from left to right along the edge in steps 1 and 2. According to the driving protocol, light is expected to move downward; however, its propagation is obstructed by the lattice edge, and upward coupling is suppressed by Zeno measurements. Consequently, light remains at this node until step 6. This behavior is confined within a unique edge Zeno subspace of unitary dimension, in contrast to the bulk Zeno subspaces $H_p^X(k)$, which have a dimension greater than one, effectively halting the system evolution (Zeno freezing). In step 6, the pathway for rightward hopping opens, allowing the light to progress to the next node along the edge. It stays at this location until step 5 of the subsequent period when the rightward pathway reopens, enabling further propagation along the edge. Across two periods, the light moves unidirectionally through four nodes. In our experiment, we fabricated an edge Zeno subspace for one step to represent the waiting process. The observed topological edge transport, illustrated in Fig. 3 (B and C), entails one-way transport of light along the lattice edge, in agreement with theoretical predictions. Upon reaching the corner, the light continues its upward journey along the right edge, where the corner (essentially a strong defect) does not scatter light backward. The opening steps are 5 for the fifth and seventh periods and 3, 7, and 8 for the sixth and eighth periods. Experimental results shown in Fig. 3 (D and E) demonstrate tight confinement along the edge with no scattering at the corner or into the bulk of the array, providing strong evidence for topological protection of the edge state.

The topological nature of this phenomenon is reflected in the inherent robustness of measurement-induced topological edge transport in the presence of structural defects and dynamic disorder, as demonstrated in Supplementary Text S5 and movies S1 to S7. We examine the effects of (i) a single missing edge site, (ii) multiple missing edge sites, and (iii) random onsite energy variations introducing both spatial and temporal disorder for both perfect and off-perfect Zeno

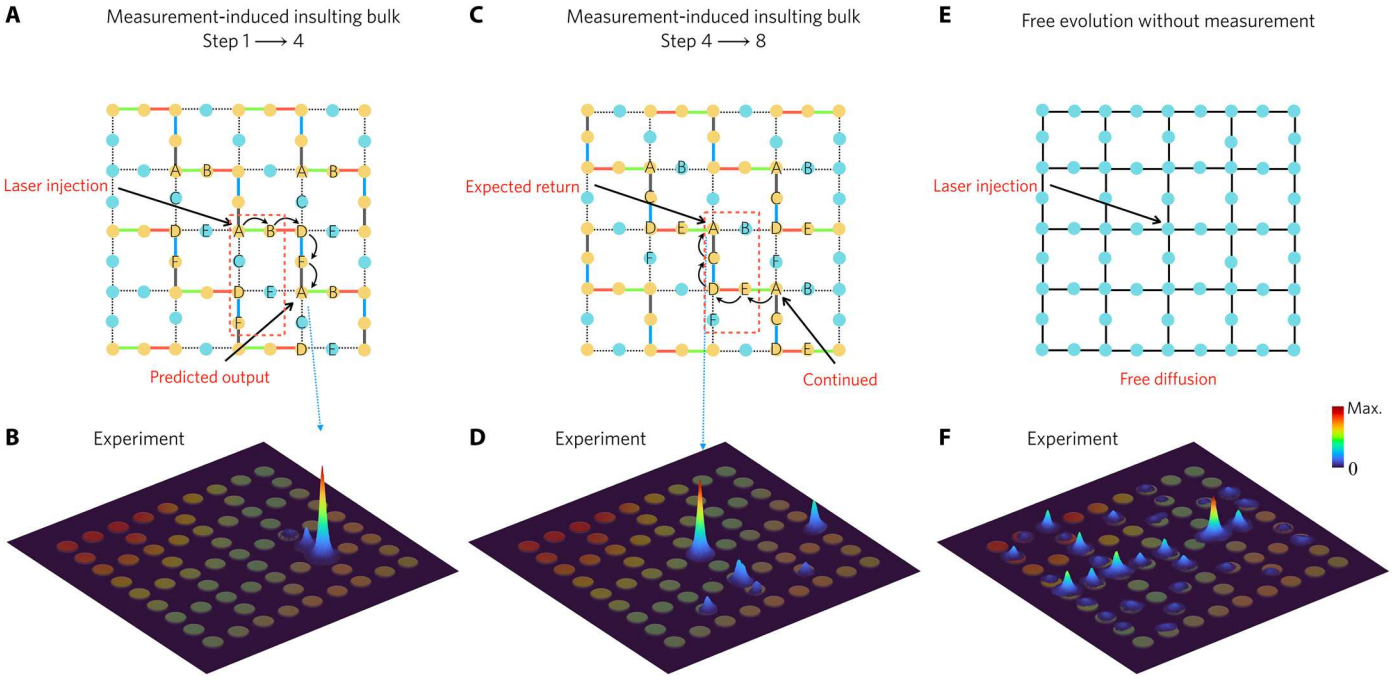

Fig. 2. Experimental observation of the measurement-induced insulating bulk inside the Lieb lattice. (**A**) Initial excitation of the lattice and predicted light trajectory for the first four-step Zeno measurements on the Lieb lattice. The lattice nodes A to F in the unit cell are marked in the figure. (**B**) Observed light distribution showing that the light is fully localized at the site diagonally opposite the injection point, consistent with the theoretical prediction. (**C**) Predicted light trajectory for the final four-step Zeno measurements in the Floquet driving protocol. (**D**) Corresponding experimental results, where light returns to the injection site, demonstrating the measurement-induced insulating bulk inside the Lieb lattice. (**E**) Schematic representation of the Lieb lattice without the measurement process, consisting solely of straight waveguides. (**F**) Experimental light distribution for the Lieb lattice without measurements. Comparison of (B), (D), and (F) illustrates that the insulating bulk in the Lieb lattice is induced by the Zeno measurements.

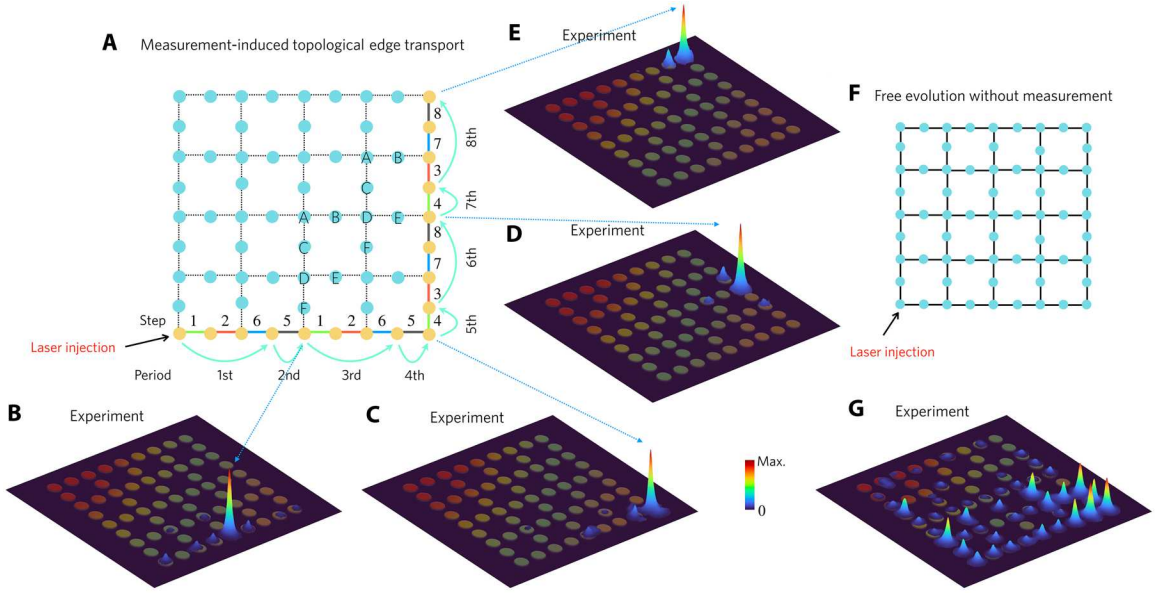

Fig. 3. Experimental results of measurement-induced unidirectional edge transport. (**A**) Light propagation trajectory along the edge of the Lieb lattice driven by Zeno measurements. The whole process encompasses eight Floquet driving periods, with the opening steps for each period illustrated. Lattice sites A to F within the unit cell are identified in the figure. (**B** to **E**) Experimentally observed unidirectional edge transport induced by the measurements on the photonic lattices. At each stage, light localizes entirely on a single lattice node. The trajectory begins along the lattice's bottom edge, navigates the corner, and ascends along the right edge, aligning with theoretical expectations. (**F**) Schematic of a standard Lieb lattice in the absence of measurements. (**G**) Experimental light distribution on a normal Lieb lattice with a laser beam introduced at the edge. The comparison between (B) through (E) and (G) demonstrates that the chiral edge transport is induced by the Zeno measurements generated by the segmented waveguide portions.

switches. When a single edge site is removed, the transport bypasses the defect without scattering into the bulk, preserving boundary propagation. Even when multiple missing edge sites are considered, light continues to propagate along the edge. Random onsite energy, induced by modifying the refractive index of the straight waveguides (including in the z direction), also does not disrupt edge transport. In the off-perfect Zeno switch, the particle diffuses to the whole lattice edge from a single-site injection. We characterize the topological transport using the edge population ratio (probability on the edge divided by total lattice probability), which remains high (~80%; fig. S12) under defects and disorder, after long propagation times (1000T, during which the particle has circled the entire edge more than 50 times). These results highlight the robustness of topologically protected edge transport, with light remaining confined to the edge despite defects and disorder, even over long propagation times. Last, for comparison, we eliminated the segmented waveguide sections, i.e., without measurements, and retain only the straight waveguides. When the lattice is excited from the same edge site, the measured light distribution, as shown in Fig. 3G, spreads throughout the entire lattice. Comparing Fig. 3 (B to E and G), it is clear that the topological edge transport is induced by Zeno measurements.

Universal lattice control using measurements

These results univocally demonstrate measurement-induced topological order through a Floquet driving protocol. The demonstrated control achieved by measurements can extend beyond the Floquet process, and the Zeno subspace can be tailored by selectively measuring specific states. Building on these insights, we propose a general formalism for achieving universal control over the lattice by precisely engineering and organizing the Zeno subspaces to meet specific requirements. Our strategy involves creating a sequence of noncommutative Zeno subspaces across the lattice. The operators governing this process can be formally expressed as $U = \prod \exp\left[-iH_p^s(k)\tau_s\right]$, where $H_p^s(k)$ represents the s-th Zeno subspace and τ_s denotes the evolution time within this subspace. This approach substantially increases the complexity of the dynamics on the lattice, surpassing the original evolution control by $H(k)$ or the Floquet driving protocol, enabling complete control over the monitored lattice. Light now evolves unitarily along the lattice under arbitrary transformations, controlled by the exponential map e^{Θ}, where Θ is an anti-Hermitian operator constructed from elements of the Lie group $\mathfrak{L}_{\text{Zeno}} = \text{Lie}_{\text{Zeno}}\{iH(k), iH_p^1(k), \cdots, iH_p^s(k), \cdots\}$. This ensures that all required transformations on the lattice can be accomplished through a sequence of Zeno measurements, allowing full control via the tailored Zeno subspaces.

As a proof of concept, we conducted a third series of experiments. Initially, three-level Zeno subspaces (yellow sites in Fig. 4A) were established by performing Zeno measurements on adjacent sites (blue sites). These subspaces are distinct from the two-level subspaces used in Floquet driving. Subsequently, a laser beam was directed into the central site of the three-level Zeno subspace. We performed 29 measurements on each measured site, corresponding to a propagation time $\tau_1 = 29(l+g) = 0.58$ cm. During this process, the single laser beam is split into two parts because of the optical Zeno effect, aligning with the experimental results shown in Fig. 4B. The split laser beam propagates upward through a double two-level Zeno subspace, as depicted in Fig. 4C. Both parts of the laser beam move simultaneously upward along the double two-level Zeno subspace without spreading to other nodes because of Zeno control, as illustrated in Fig. 4D. This setup effectively realizes a measurement-induced

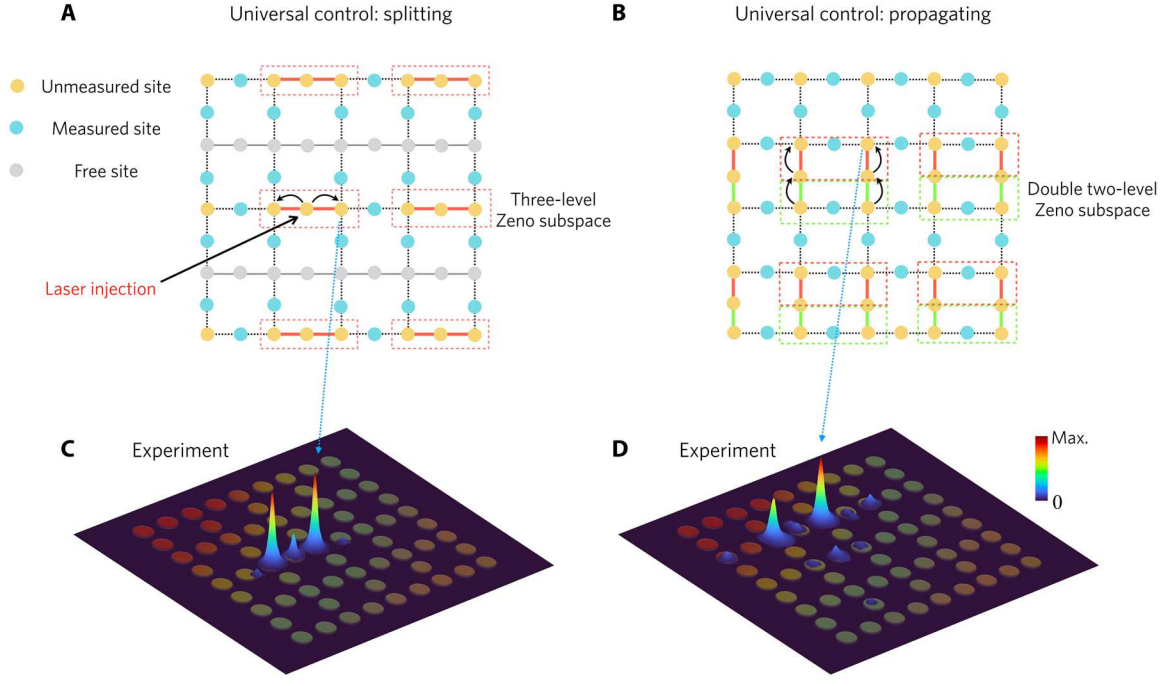

Fig. 4. Experimental observation of the beam splitter in the Lieb lattice generated by measurements. (**A**) Illustration of the measured nodes (blue) and unmeasured nodes for the generation of three-level Zeno subspaces in the Lieb lattice. (**B**) Experimental light distribution for splitting the laser beam using the Zeno subspace. The injected laser beam is split into two parts, consistent with the theoretical predictions. (**C**) Upward propagation of the split laser beam using double two-level Zeno subspaces. (**D**) Experimental light output after two steps of upward propagation operations. This demonstrates the measurement-induced beam splitter inside the Lieb lattice.

in-lattice beam splitter, demonstrating the potential for precise and universal lattice control through the strategic use of measurement processes. Our results generally demonstrate that we can generate complex dynamics on a lattice by designing Zeno subspaces on demand, inducing topological transitions, modifying photon transport, and designing ad hoc scattering features.

DISCUSSION

In this work, we have introduced and experimentally demonstrated measurement-induced topological transitions in photonic lattices, illustrating how measurements can serve as a powerful tool to drive a topologically trivial lattice into a topological phase. Our work establishes measurement backaction as a general external mechanism to dynamically engineer topological matter—an avenue that has not been explored in any prior studies of topology. The experiments, although realized in a photonic platform with classic light excitations, when mapped back onto a quantum measurement system, demonstrate that our protocol provides a way to induce topological order through a sequence of quantum measurements, establishing measurements as unique tools for generating topology in quantum matter. Consequently, our results suggest implications for both photonics and quantum physics. From a technological perspective, the segmented waveguide we design can effectively pause light for programmable durations and thus can act as an optical "memory" element. In addition, although we use the Lieb lattice for our demonstration, the proposed protocol can be adapted to other lattice geometries. Notably, our approach enables exquisite dynamic control of topological order without perturbing the lattice geometry, but simply by introducing broken symmetry and Floquet phases through the measurement protocol itself, in a precise and dynamic fashion. This concept paves the way for exploring the rich interplay between the lattice structure, measurements, and topology in integrated photonics.

Beyond inducing topological transitions, our work also shows that the measurement process can perform complex operations on a photonic lattice, another concept that we proposed and validated experimentally in this work. By generating different noncommutative Zeno subspaces, we can achieve dynamic and universal control over the lattice. This capability allows exploring a variety of measurement-induced phenomena in photonics and designing compact, functional devices within photonic lattices. For example, we can first perform a topological edge transport on the lattice and then precisely control its pathway to a specific target or split it into pieces (as our third experiment showed) using this universal control on the lattice.

Even though our experiments were conducted within a photonic framework, the underlying measurement protocol is extendable to other platforms, such as acoustics, electronic circuits, or cold atoms, and to quantum platforms. Consequently, our work not only introduces a distinct strategy for designing topological insulators but also paves the way for designing tunable on-chip devices, leveraging on-demand measurement-based control both for classical and quantum platforms.

MATERIALS AND METHODS

Experimental design

Fabrication of the 3D waveguide array

The photonic waveguide structures used in this work are fabricated in commercially available borosilicate glass (Eagle XG) using the well-developed technique of direct femtosecond laser writing. The glass is mounted on a computer-controlled three-dimensional (3D) *x*-*y*-*z* translation stage (Hybrid Hexapod, ALIO). A femtosecond laser (Femto YL-25, YSL Photonics) at the wavelength of 1030 nm, the pulse duration of 400 fs, and the repetition rate of 2.5 MHz is used as the light source. A microscope objective [50×/0.45 numerical aperture (NA)] is used to focus the laser beam below the substrate surface of the sample. The pulse energy is adjusted to ~152 nJ, and the writing speed is set to 1 mm s^{-1}. Laser writing produces typical type I waveguides with a width of ~4 μm, and the refractive index difference Δn between waveguide cores and cladding is ~10^{-3}.

End-face coupling system

The characterization of the waveguide system is performed by an end-face coupling system, illustrated in fig. S1. The laser with the wavelength of 532 nm is injected into the selected waveguide of the system by a microscope objective (20×/0.4 NA) to excite waveguide modes. The output intensity distribution (beam evolution) is measured (monitored) at the output facet using a charge-coupled device camera by another microscope objective (20×/0.4 NA). In addition, the morphology of the structural end facets is assessed using a metalloscope (Axio Imager, Carl Zeiss).

Characterization of coupling strength in waveguide arrays

Before conducting the main experiment, we first quantify the coupling strength as a function of the distance between two aligned waveguides using the fabricated waveguide structures. We initiated the excitation of two coupled waveguides from WG1 with a 532-nm laser beam and varied the distance d between them (see fig. S2A). The light intensity along the waveguide, described by $I = I_0 \sin^2(\kappa l)$, where κ represents the coupling magnitude and l the propagation length in the z direction, was measured. The coupling magnitude κ was experimentally determined for various distances d, as shown in fig. S2B. We then fit the data to an exponential function to establish the relationship between the distance d and the coupling magnitude, which informed subsequent experiments.

We further investigated whether the writing depth influences the waveguides' coupling properties. The initial experiments were performed at a fabrication depth of 112.5 μm in the y direction. We then repeated the procedure at a depth of 225 μm. The experimentally derived coupling magnitudes, also presented in fig. S2B, indicate that the writing depth does not affect the coupling properties. This finding allowed us to proceed with fabricating 3D waveguide structures for further experiments.

Supplementary Materials

The PDF file includes:

Supplementary Text
Figs. S1 to S12
Table S1
Legends for movies S1 to S7

Other Supplementary Material for this manuscript includes the following:

Movies S1 to S7

REFERENCES AND NOTES

1. M. Z. Hasan, C. L. Kane, Colloqium: Topological insulators. *Rev. Mod. Phys.* **82**, 3045–3067 (2010).
2. K. V. Klitzing, G. Dorda, M. Pepper, New method for high-accuracy determination of the fine-structure constant based on quantized Hall resistance. *Phys. Rev. Lett.* **45**, 494–497 (1980).
3. C. L. Kane, E. J. Mele, Quantum spin Hall effect in graphene. *Phys. Rev. Lett.* **95**, 226801 (2005).
4. C. L. Kane, E. J. Mele, Z_2 topological order and the quantum spin Hall effect. *Phys. Rev. Lett.* **95**, 146802 (2005).

5. B. A. Bernevig, S. C. Zhang, Quantum spin Hall effect. *Phys. Rev. Lett.* **96**, 106802 (2006).
6. M. König, S. Wiedmann, C. Brüne, A. Roth, H. Buhmann, L. W. Molenkamp, X.-L. Qi, S.-C. Zhang, Quantum spin Hall insulator state in HgTe quantum wells. *Science* **318**, 766–770 (2007).
7. D. Hsieh, D. Qian, L. Wray, Y. Xia, Y. S. Hor, R. J. Cava, M. Z. Hasan, A topological Dirac insulator in a quantum spin Hall phase. *Nature* **452**, 970–974 (2008).
8. Z. Wang, Y. Chong, J. D. Joannopoulos, M. Soljacic, Observation of unidirectional backscattering-immune topological electromagnetic states. *Nature* **461**, 772–775 (2009).
9. G. Jotzu, M. Messer, R. Desbuquois, M. Lebrat, T. Uehlinger, D. Greif, T. Esslinger, Experimental realization of the topological Haldane model with ultracold fermions. *Nature* **515**, 237–240 (2014).
10. X. Ni, M. Weiner, A. Alu, A. B. Khanikaev, Observation of higher-order topological acoustic states protected by generalized chiral symmetry. *Nat. Mater.* **18**, 113–120 (2019).
11. Y. Hadad, J. C. Soric, A. B. Khanikaev, A. Alu, A., Self-induced topological protection in nonlinear circuit arrays. *Nat. Electron.* **1**, 178–182 (2018).
12. M. C. Rechtsman, J. M. Zeuner, Y. Plotnik, Y. Lumer, D. Podolsky, F. Dreisow, S. Nolte, M. Segev, A. Szameit, Photonic Floquet topological insulators. *Nature* **496**, 196–200 (2013).
13. L. Lu, J. D. Joannopoulos, M. Soljacic, Topological photonics. *Nat. Photon.* **8**, 821–829 (2014).
14. T. Ozawa, H. M. Price, A. Amo, N. Goldman, M. Hafezi, L. Lu, M. C. Rechtsman, D. Schuster, J. Simon, O. Zilberberg, I. Carusotto, Topological photonics. *Rev. Mod. Phys.* **91**, 015006 (2019).
15. M. Li, D. Zhirihin, M. Gorlach, X. Ni, D. Filonov, A. Slobozhanyuk, A. Alù, A. B. Khanikaev, Higher-order topological states in photonic kagome crystals with long-range interactions. *Nat. Photonics* **14**, 89–94 (2020).
16. S. Weidemann, M. Kremer, T. Helbig, T. Hofmann, A. Stegmaier, M. Greiter, R. Thomale, A. Szameit, Topological funneling of light. *Science* **368**, 311–314 (2020).
17. S. Guddala, F. Komissarenko, S. Kiriushechkina, A. Vakulenko, M. Li, V. M. Menon, A. Alù, A. B. Khanikaev, Topological phonon-polariton funneling in midinfrared metasurfaces. *Science* **374**, 225–227 (2021).
18. S. Xia, D. Kaltsas, D. Song, I. Komis, J. Xu, A. Szameit, H. Buljan, K. G. Makris, Z. Chen, Nonlinear tuning of PT symmetry and non-Hermitian topological states. *Science* **372**, 72–76 (2021).
19. G. Harari, M. A. Bandres, Y. Lumer, M. C. Rechtsman, Y. D. Chong, M. Khajavikhan, D. N. Christodoulides, M. Segev, Topological insulator laser: Theory. *Science* **359**, eaar4003 (2018).
20. M. A. Bandres, S. Wittek, G. Harari, M. Parto, J. Ren, M. Segev, D. N. Christodoulides, M. Khajavikhan, Topological insulator laser: Experiments. *Science* **359**, eaar4005 (2018).
21. S. Weimann, M. Kremer, Y. Plotnik, Y. Lumer, S. Nolte, K. G. Makris, M. Segev, M. C. Rechtsman, A. Szameit, Topologically protected bound states in photonic parity–time-symmetric crystals. *Nat. Mater.* **16**, 433–438 (2017).
22. L. J. Maczewsky, M. Heinrich, M. Kremer, S. K. Ivanov, M. Ehrhardt, F. Martinez, Y. V. Kartashov, V. V. Konotop, L. Torner, D. Bauer, A. Szameit, Nonlinearity-induced photonic topological insulator. *Science* **370**, 701–704 (2020).
23. M. S. Rudner, N. H. Lindner, E. Berg, M. Levin, Anomalous edge states and the bulk-edge correspondence for periodically driven two-dimensional systems. *Phys. Rev. X* **3**, 031005 (2013).
24. R. Fleury, A. B. Khanikaev, A. Alù, A., Floquet topological insulators for sound. *Nat. Commun.* **7**, 1–11 (2016).
25. L. J. Maczewsky, J. M. Zeuner, S. Nolte, A. Szameit, Observation of photonic anomalous Floquet topological insulators. *Nat. Commun.* **8**, 13756 (2017).
26. S. Mukherjee, M. C. Rechtsman, Observation of Floquet solitons in a topological bandgap. *Science* **368**, 856–859 (2020).
27. A. Nagulu, X. Ni, A. Kord, M. Tymchenko, S. Garikapati, A. Alù, H. Krishnaswamy, Chip-scale Floquet topological insulators for 5G wireless systems. *Nat. Electron.* **5**, 300–309 (2022).
28. G. G. Pyrialakos, J. Beck, M. Heinrich, L. J. Maczewsky, N. V. Kantartzis, S. Weidemann, A. Szameit, D. N. Christodoulides, Bimorphic Floquet topological insulators. *Nat. Mater.* **21**, 634–639 (2022).
29. A. Fritzsche, T. Biesenthal, L. J. Maczewsky, K. Becker, M. Ehrhardt, M. Heinrich, R. Thomale, Y. N. Joglekar, A. Szameit, Parity–time-symmetric photonic topological insulator. *Nat. Mater.* **23**, 377–382 (2024).
30. L. J. Maczewsky, B. Höckendorf, M. Kremer, T. Biesenthal, M. Heinrich, A. Alvermann, H. Fehske, A. Szameit, Fermionic time-reversal symmetry in a photonic topological insulator. *Nat. Mater.* **19**, 855–860 (2020).
31. Q. Chen, Z. Zhang, H. Qin, A. Bossart, Y. Yang, H. Chen, R. Fleury, Anomalous and Chern topological waves in hyperbolic networks. *Nat. Commun.* **15**, 2293 (2024).
32. Z. Zhang, P. Delplace, R. Fleury, Superior robustness of anomalous non-reciprocal topological edge states. *Nature* **598**, 293–297 (2021).
33. H. M. Wiseman, G. J. Milburn, *Quantum Measurement and Control* (Cambridge Univ. Press, Cambridge, 2011).
34. Y.-W. Cho, Y. Kim, Y.-H. Choi, Y.-S. Kim, S.-W. Han, S.-Y. Lee, S. Moon, Y.-H. Kim, Emergence of the geometric phase from quantum measurement back-action. *Nat. Phys.* **15**, 665–670 (2019).
35. C. H. Bennett, G. Brassard, C. Crépeau, R. Jozsa, A. Peres, W. K. Wootters, Teleporting an unknown quantum state via dual classical and Einstein-Podolsky-Rosen channels. *Phys. Rev. Lett.* **70**, 1895–1899 (1993).
36. H. J. Briegel, D. E. Browne, W. Dür, R. Raussendorf, M. Van den Nest, Measurement-based quantum computation. *Nat. Phys.* **5**, 19–26 (2009).
37. T. Brydges, A. Elben, P. Jurcevic, B. Vermersch, C. Maier, B. P. Lanyon, P. Zoller, R. Blatt, C. F. Roos, Probing Rényi entanglement entropy via randomized measurements. *Science* **364**, 260–263 (2019).
38. B. Skinner, J. Ruhman, A. Nahum, Measurement-induced phase transitions in the dynamics of entanglement. *Phys. Rev. X* **9**, 031009 (2019).
39. M. Wampler, B. J. J. Khor, G. Refael, I. Klich, Stirring by staring: Measurement-induced chirality. *Phys. Rev. X* **12**, 031031 (2022).
40. A. I. Google Quantum, Collaborators., Measurement-induced entanglement and teleportation on a noisy quantum processor. *Nature* **622**, 481–486 (2023).
41. J. M. Raimond, C. Sayrin, S. Gleyzes, I. Dotsenko, M. Brune, S. Haroche, P. Facchi, S. Pascazio, Phase space tweezers for tailoring cavity fields by quantum Zeno dynamics. *Phys. Rev. Lett.* **105**, 213601 (2010).
42. G. Barontini, L. Hohmann, F. Haas, J. Estève, J. Reichel, Deterministic generation of multiparticle entanglement by quantum Zeno dynamics. *Science* **349**, 1317–1321 (2015).
43. B. Misra, E. C. G. Sudarshan, The Zeno's paradox in quantum theory. *J. Math. Phys.* **18**, 756–763 (1977).
44. W. M. Itano, D. J. Heinzen, J. J. Bollinger, D. J. Wineland, Quantum Zeno effect. *Phys. Rev. A* **41**, 2295–2300 (1990).
45. P. Facchi, S. Pascazio, Quantum Zeno dynamics: Mathematical and physical aspects. *J. Phys. A: Math. Theor.* **41**, 493001 (2008).
46. P. Facchi, H. Nakazato, S. Pascazio, From the quantum Zeno to the inverse quantum Zeno effect. *Phys. Rev. Lett.* **86**, 2699–2703 (2001).
47. E. W. Streed, J. Mun, M. Boyd, G. K. Campbell, P. Medley, W. Ketterle, D. E. Pritchard, Continuous and pulsed quantum Zeno effect. *Phys. Rev. Lett.* **97**, 260402 (2006).
48. P. Facchi, S. Pascazio, Quantum Zeno subspaces. *Phys. Rev. Lett.* **89**, 080401 (2002).
49. F. Schäfer, I. Herrera, S. Cherukattil, C. Lovecchio, F. S. Cataliotti, F. Caruso, A. Smerzi, Experimental realization of quantum Zeno dynamics. *Nat. Commun.* **5**, 3194 (2014).
50. A. Signoles, A. Facon, D. Grosso, I. Dotsenko, S. Haroche, J.-M. Raimond, M. Brune, S. Gleyzes, Confined quantum Zeno dynamics of a watched atomic arrow. *Nat. Phys.* **10**, 715–719 (2014).
51. S. Longhi, Nonexponential decay via tunneling in tight-binding lattices and the optical Zeno effect. *Phys. Rev. Lett.* **97**, 110402 (2006).
52. F. Dreisow, A. Szameit, M. Heinrich, T. Pertsch, S. Nolte, A. Tünnermann, S. Longhi, Decay control via discrete-to-continuum coupling modulation in an optical waveguide system. *Phys. Rev. Lett.* **101**, 143602 (2008).
53. P. Biagioni, G. Della Valle, M. Ornigotti, M. Finazzi, L. Duò, P. Laporta, S. Longhi, Experimental demonstration of the optical Zeno effect by scanning tunneling optical microscopy. *Opt. Express* **16**, 3762–3767 (2008).
54. K. T. McCusker, Y.-P. Huang, A. S. Kowligy, P. Kumar, Experimental demonstration of interaction-free all-optical switching via the quantum Zeno effect. *Phys. Rev. Lett.* **110**, 240403 (2013).
55. X. Guo, C.-L. Zou, L. Jiang, H. X. Tang, All-optical control of linear and nonlinear energy transfer via the Zeno effect. *Phys. Rev. Lett.* **120**, 203902 (2018).
56. A. Crespi, F. V. Pepe, P. Facchi, F. Sciarrino, P. Mataloni, H. Nakazato, S. Pascazio, R. Osellame, Experimental investigation of quantum decay at short, intermediate, and long times via integrated photonics. *Phys. Rev. Lett.* **122**, 130401 (2019).
57. Z.-X. Huang, H.-W. Wu, L.-L. Cheng, P.-X. Xie, X. Chen, H.-F. Xu, Z.-Q. Sheng, Steering sound propagation with Zeno barriers in acoustic waveguide arrays. *Appl. Phys. Lett.* **125**, 152201 (2024).
58. X.-M. Zhang, Z.-G. Chen, G. Ma, M.-H. Lu, Y.-F. Chen, Zeno freezing and anti-Zeno acceleration of the dynamic evolution of acoustic topological boundary states. arXiv:2501.03502 (2025). https://doi.org/10.48550/arXiv.2501.03502.
59. M.-A. Miri, A. Alù, Exceptional points in optics and photonics. *Science* **363**, eaar7709 (2019).
60. L. Feng, R. El-Ganainy, L. Ge, Non-Hermitian photonics based on parity-time symmetry. *Nat. Photon.* **11**, 752–762 (2017).
61. A. Szameit, S. Nolte, Discrete optics in femtosecond-laser-written photonic structures. *J. Phys. B* **43**, 163001 (2010).
62. M. R. Slot, T. S. Gardenier, P. H. Jacobse, G. C. P. van Miert, S. N. Kempkes, S. J. M. Zevenhuizen, C. Morais Smith, D. Vanmaekelbergh, I. Swart, Experimental realization and characterization of an electronic Lieb lattice. *Nat. Phys.* **13**, 672–676 (2017).

63. Y. V. Kartashov, V. A. Vysloukh, L. Torner, Resonant mode oscillations in modulated waveguiding structures. *Phys. Rev. Lett.* **99**, 233903 (2007).
64. M. Ornigotti, G. Della Valle, T. T. Fernandez, A. Coppa, V. Foglietti, P. Laporta, S. Longhi, Visualization of two-photon Rabi oscillations in evanescently coupled optical waveguides. *J. Phys. B: At. Mol. Opt. Phys.* **41**, 085402 (2008).

Acknowledgments

Funding: This work was supported by the following: National Natural Science Foundation of China (12361141815), National Natural Science Foundation of China (12174222), Natural Science Foundation of Shandong Province (ZR2021ZD02), Taishan Scholars Programme of Shandong Province (tspd20210303), Julian Schwinger Foundation for Physics Research, and Simons Foundation. **Author contributions:** Conceptualization: F.C. and A.A. Methodology: A.A., K.Z., and F.C. Investigation: Q.L., W.L., K.Z., F.C., A.A., and Y.J. Visualization: Q.L. and W.L. Funding acquisition: F.C., A.A., and K.Z. Project administration: F.C. and A.A. Supervision: F.C. and A.A. Writing—original draft: Q.L., W.L., and K.Z. Writing—review and editing: A.A. and F.C. **Competing interests:** The authors declare that they have no competing interests. **Data and materials availability:** All data needed to evaluate the conclusions in the paper are present in the paper and/or the Supplementary Materials.

Submitted 26 February 2025
Accepted 16 June 2025
Published 18 July 2025
10.1126/sciadv.adx0595